Euro. Jnl of Applied Mathematics (1999), *vol.* 10, *pp.* 297–318. Printed in the United Kingdom

Numerical and asymptotic results on the linear stability of a thin film spreading down a slope of small inclination

A. MÜNCH and B. A. WAGNER

Zentrum Mathematik (H4), Lehrstuhl für Angewandte Mathematik,
Technische Universität München, Arcisstraße 21, 80290 München, Germany

(*Received 17 November 1997; revised 6 January 1999*)

We model a thin liquid film moving down a slope using the lubrication approximation with a slip condition. The travelling-wave solution is derived for small inclination angle α, using singular perturbation methods, and compared to the numerical solution. For the linear stability analysis we combine numerical methods with the long-wave approximation and find a small but finite critical α^* below which the flow remains linearly stable to spanwise perturbations. This is contrasted with the vanishing of the hump of the travelling-wave solution. Finally, the prevailing linear stability of the travelling-wave at small inclination angles is compared with recent related results using a precursor model. Here, though, a strong dependence on the magnitude of the contact angle is found, which we think has not been observed before.

1 Introduction

The control of the behaviour of the three-phase contact line of a thin spreading fluid sheet is most important in many industrial coating processes. Yet the modelling of the three-phase contact line still remains physically unclear, as do the mechanisms underlying the eventual development of instabilities, such as finger or sawtooth patterns.

One of the first people to observe these phenomena experimentally was Huppert [1], and many researchers have investigated them since. As can be seen from further experimental work by Silvi & Dussan [2], Jerrett & de Bruyn [3], de Bruyn [4], Schwartz & Tejada [5] and Johnson *et al.* [6], accurate measurements of fluid properties such as fluid depth, dynamic contact angle or contact line velocity of a moving fluid sheet present difficulties, in particular during the onset of the instability, as well as for small inclination angles.

Qualitatively, just before the onset of the instability a hump close to the contact line is observed and, depending whether the size of the contact angle is small or large, either sawtooth patterns or finger patterns evolve. The main difference between these patterns are that sawtooth patterns eventually lead to a complete coating, while finger patterns leave dry or uncoated regions, the prediction and simulation of which may be important for industrial applications.

One of the first people to model the spreading of a thin fluid driven by gravity was Greenspan [7], who used the thinness of the film to derive the simpler yet still nonlinear lubrication approximation as the leading order problem for small capillary numbers; he

also introduced a slip function such that no singularity in the governing equation for the height of the film occurs at the contact line. He also used a contact angle model that for small front velocities yields a linear relationship between the slip velocity and the contact angle. Further studies, by slightly varying the contact angle model and slip function were done by Hocking [8], Cazabat *et al.* [9], Goodwin & Homsey [10], Hocking & Miksis [11] and Miksis *et al.* [12]. On the other hand, precursor models, where the narrow region connecting a very thin film in front of the relatively thicker fluid sheet replaces the contact line, have been investigated by Troian *et al.* [13] and Bertozzi & Brenner [14]. Both models predict a preferred wavelength of the linear stability to spanwise perturbations of the leading front and find good qualitative agreement in comparison to experiments.

In our analysis we use a slip model and compare to recent predictions of Bertozzi & Brenner [14]. There, a critical inclination angle α^* was found below which the flow remained linearly stable. However, α^* was above the inclination angles for which instabilities still occur in experiments [14].

In the linear stability analysis of our model a critical inclination angle α^* is also found; it depends strongly on the value of the contact angle and becomes smaller for larger contact angles. Similarly, there is a critical α, also dependent on the contact angle, at which the hump of the fluid sheet vanishes. Both functions are compared and discussed. For these (typically) small inclination angles, numerical simulation becomes increasingly difficult. On the other hand, the fastest growing mode becomes very small in that range, so that it becomes useful to perform a long-wave analysis of the resulting eigenvalue problem. By improving our numerical code to a degree of accuracy where the growth rates overlap with those predicted by the long-wave analysis, we obtain also in this extended range of small α the growth rate as a function of the wave number for the complete range of wave numbers.

Furthermore, the value of the growth rate in our long-wave analysis depends only on the behaviour of the nonlinear base state of the problem, i.e. the travelling-wave solution. This however can be derived analytically via matched asymptotics for small inclination angles, and good agreement with the numerical solution is found.

In this study, we first use singular perturbation methods to derive the travelling-wave solution and compare it to our numerical solution. Next we study the spanwise linear stability of this solution both numerically and then using long-wave analysis. Finally, these results are used to discuss linear stability for small but finite α.

2 Formulation

Let a thin liquid film initially move uniformly on a plane inclined at an angle α to the horizontal as depicted in Figure 1. In coordinates (x, y, z) the liquid-gas interface is located at $z = h(x, y, t)$, z being perpendicular to the plane, and x and y in the plane, with x pointing in the downstream direction. The velocity is $\boldsymbol{u} = (u, v, w)$.

The bulk of the liquid is governed by the continuity and Navier–Stokes equations:

$$\nabla \cdot \boldsymbol{u} = 0, \tag{2.1}$$

$$\rho \{u_t + (\boldsymbol{u} \cdot \nabla)\boldsymbol{u}\} = \rho \boldsymbol{g} - \nabla p + \mu \Delta \boldsymbol{u}, \tag{2.2}$$

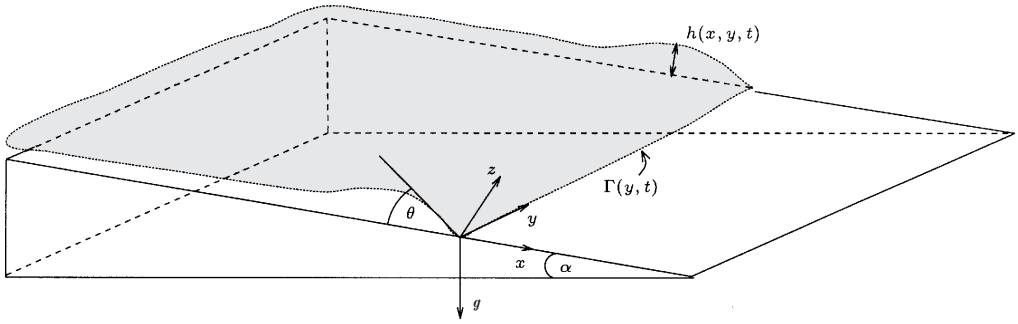

FIGURE 1. A sheet of fluid spreading over a slope.

where ρ, p and μ are the density, the pressure and the viscosity of the fluid, respectively, $\boldsymbol{g} = (g\sin\alpha, 0, -g\cos\alpha)$ and g is the gravitational constant.

The equations at the liquid-gas interface are the kinematic condition, continuity of tangential stress and the pressure jump:

$$h_t + h_x u + h_y v = w, \tag{2.3}$$

$$\boldsymbol{t}_j \cdot \Pi \cdot \boldsymbol{n} = 0, \tag{2.4}$$

$$p(x, y, h(x, y, t)) - p_A = \boldsymbol{n} \cdot \Pi \cdot \boldsymbol{n} - \sigma \nabla \cdot \left(\frac{\nabla h}{\sqrt{1 + h_x^2 + h_y^2}} \right), \tag{2.5}$$

with the surface normal

$$\boldsymbol{n} = \frac{(-h_x, -h_y, 1)}{\sqrt{1 + h_x^2 + h_y^2}},$$

and tangents

$$\boldsymbol{t}_j = \frac{(\delta_{1j}, \delta_{2j}, h_{x_j})}{\sqrt{1 + h_{x_j}^2}} \qquad j = 1, 2,$$

where Π is the Newton stress tensor, σ is the surface tension coefficient, p_A the outside pressure (e.g. of air) and δ_{kj} are the Kronecker delta symbols.

At the surface of the plate, we require impermeability and allow for a slip in order to avoid the stress singularity at the moving contact line:

$$w|_{z=0} = 0, \tag{2.6}$$

$$(u, v)|_{z=0} = \frac{\lambda}{h} \; (u_z, v_z)|_{z=0}, \qquad \lambda = \text{const.} \tag{2.7}$$

The slip-law we use here assumes that the slip coefficient is directly proportional to the local thickness of the film. Since λ is of microscopic size, λ/h is negligible except near the contact line. It goes back to the well-known model by Greenspan [7] for the spreading of thin liquid drops. Miksis *et al.* [12] used this law for the spreading of thin liquid films and compared it to recent experiments by Johnson *et al.* [6]. Very similar slip conditions are also used by Dussan [15]. A derivation of an effective slip of this form from a microscopic model can be found in Neogi & Miller [16]. Their model assumes a rough solid surface and uses results based on experimental investigations by Beavers & Joseph

[17] and Taylor & Richardson [18, 19]. For comparisons of (2.7) with other slip-laws and their effect on spreading rates, see also Haley & Miksis [20].

At the contact line itself, the height of the film is zero:

$$h|_\Gamma = 0. \tag{2.8}$$

For the dynamic contact angle, there are a variety of models in the literature [5, 7, 11, 12, 22]. We restrict ourselves to sufficiently small static and dynamic contact angles and capillary numbers, so that the lubrication assumption remains valid (see Goodwin & Homsy [10]). Hence, for our situation we will choose, on the basis of the model of Blake & Haynes [23], a linear relationship between the contact angle θ, which is the angle between the tangent to the free surface and the plane in a plane normal to $\Gamma(y,t)$, and the velocity at the contact line as a first approximation:

$$(u,v)|_\Gamma \cdot \boldsymbol{n}_\Gamma = \kappa(\theta - \theta_S),$$

where θ_S is the static contact angle and κ is a constant.

We can relate the slip velocity on the left-hand side and the contact angle through

$$\Gamma_t + \Gamma_y\, v|_\Gamma = u|_\Gamma\,,$$
$$\boldsymbol{n}_\Gamma = \tfrac{(1,-\Gamma_y)}{\sqrt{1+\Gamma_y^2}},$$

and

$$\left.\frac{\partial h}{\partial n_\Gamma}\right|_\Gamma = -\tan\theta(y,t),$$

so that we are left with

$$\frac{\Gamma_t}{\sqrt{1+\Gamma_y^2}} = \kappa(\theta - \theta_S), \tag{2.9}$$

and

$$\left.\frac{h_x - h_y\Gamma_y}{\sqrt{1+\Gamma_y^2}}\right|_\Gamma = -\tan\theta(y,t). \tag{2.10}$$

Far upstream we let the height of the film $h(x,y,t)$ be uniform, i.e.:

$$\lim_{x\to-\infty} h(x,y,t) = h_\infty, \tag{2.11}$$

$$\lim_{x\to-\infty} \frac{\partial^v h}{\partial x^v}(x,y,t) = 0, \qquad v \in \mathbb{N}. \tag{2.12}$$

The fluid is driven at a constant flow-rate Q_∞ at $x = -\infty$

$$Q_\infty = \frac{\rho g h_\infty^3}{3\mu}\left(1 + 3\frac{\lambda}{h_\infty^2}\right)\sin\alpha,$$

so that

$$V = \frac{Q_\infty}{h_\infty} = \frac{\rho g h_\infty^2}{3\mu}\left(1 + 3\frac{\lambda}{h_\infty^2}\right)\sin\alpha\,, \tag{2.13}$$

for a given inclination angle α.

By introducing the scales

$$\left.\begin{aligned} x &= l\hat{x}, & y &= l\hat{y}, & \Gamma &= l\hat{\Gamma}, \\ z &= h_\infty \hat{z}, & h &= h_\infty \hat{h}, & \theta &= \frac{h_\infty}{l}\hat{\theta}, \\ u &= V\hat{u}, & v &= V\hat{v}, & w &= \frac{h_\infty}{l}V\hat{w}, \\ t &= \frac{l}{V}\hat{t}, & p - p_A &= \frac{\sigma h_\infty}{l^2}\hat{p}, & \theta_S &= \frac{h_\infty}{l}\hat{\theta}_S. \end{aligned}\right\} \tag{2.14}$$

a lubrication approximation for (2.1)–(2.12) is frequently derived by requiring

$$\frac{h_\infty}{l} = \mathrm{Ca}^{1/3} \ll 1, \tag{2.15}$$

where $\mathrm{Ca} = 3\mu V/\sigma$ is the capillary number [7, 13, 12]. If only the leading order terms in $\mathrm{Ca}^{1/3}$ are retained, the resulting equations can then be integrated across the height of the film h, and by applying the kinematic condition, a nonlinear evolution equation for the shape of the fluid film is obtained,

$$h_t = -\nabla \cdot \left[\left(h^3 + d^2 h\right) \left(\nabla \Delta h - G \nabla h + \frac{1}{1+d^2}(1,0)^T \right) \right], \tag{2.16}$$

$\left(\nabla = \left(\frac{\partial}{\partial x}, \frac{\partial}{\partial y} \right), \Delta = \frac{\partial^2}{\partial x^2} + \frac{\partial^2}{\partial y^2} \right)$ together with the boundary conditions

$$h|_\Gamma = 0, \tag{2.17}$$

$$\left. \frac{\Gamma_t}{\sqrt{1+\Gamma_y^2}} \right|_\Gamma = \frac{1}{D}(\theta - \theta_S), \tag{2.18}$$

$$\left. \frac{h_x - h_y \Gamma_y}{\sqrt{1+\Gamma_y^2}} \right|_\Gamma = -\theta, \tag{2.19}$$

$$\lim_{x \to -\infty} h(x,y,t) = 1, \tag{2.20}$$

$$\lim_{x \to -\infty} \frac{\partial^n}{\partial x^n} h(x,y,t) = 0, \qquad n \in \mathbb{N}, \tag{2.21}$$

where the '^'s have been dropped, and where $D = Vl/\kappa h_\infty$ and $G = \mathrm{Ca}^{1/3} \cot\alpha/(1+d^2)$ are $O(1)$ or smaller. In our subsequent calculations, typical choices for the scaled slip-coefficient $d^2 = 3\lambda/h_\infty^2$ will be in the range of $0.0001 \ldots 0.03$.

In this study, we are interested in the case $\alpha \ll 1$. However, this scaling forces the parallel component of gravity to enter as an $O(1)$-term, which is not what one would expect for a just slightly inclined plane. For such a situation, a more suitable scaling, which allows this component to enter as a small correction, is given as follows:

$$\begin{aligned} x &= x_0 x^+, & y &= x_0 y^+, & z &= h_\infty z^+, \\ u &= V u^+, & v &= V v^+, & w &= \frac{h_\infty V}{x_0} w^+, \\ h &= h_\infty h^+, & t &= \frac{x_0}{V} t^+, & p - p_A &= \rho g h_\infty p^+, \\ \Gamma &= x_0 \Gamma^+, & \theta &= \frac{h_\infty}{x_0}\theta^+, & \theta_S &= \frac{h_\infty}{x_0}\theta_S^+. \end{aligned}$$

Upon substitution into (2.1)–(2.12) a lubrication approximation is obtained if $\epsilon = h_\infty/x_0 \ll 1$, and if for $\alpha \ll 1$ (i.e. $\sin\alpha \sim \alpha + O(\alpha^3)$ and $\cos\alpha \sim 1 + O(\alpha^2)$) the parameter $v = \alpha/\epsilon$ is at most $O(1)$. To include surface tension effects, the Bond number $B = \rho g x_0^2/\sigma = O(1)$.

After dropping the '+'s, we proceed as usual and integrate the resulting equations across the height h. In conjunction with the kinematic condition, we obtain the problem

$$v(1+d^2)\,h_t = -\nabla\cdot\left[(h^3 + d^2\,h)\left(\frac{1}{B}\nabla\Delta h - \nabla h + (v,0)^T\right)\right], \tag{2.22}$$

with boundary conditions

$$h|_\Gamma = 0, \tag{2.23}$$

$$\frac{v\Gamma_t}{\sqrt{1+\Gamma_y^2}} = \frac{1}{D_1}(\theta - \theta_S) \quad \text{with} \quad D_1 = \frac{\rho g h_\infty^2}{3\mu\kappa}(1+d^2) = O(1), \tag{2.24}$$

$$\frac{h_x - h_y\Gamma_y}{\sqrt{1+\Gamma_y^2}} = -\theta, \tag{2.25}$$

$$\lim_{x\to-\infty} h(x,y,t) = 1, \tag{2.26}$$

$$\lim_{x\to-\infty} \frac{\partial^n}{\partial x^n} h(x,y,t) = 0, \qquad n \in \mathbb{N}. \tag{2.27}$$

3 The travelling-wave solution

For the problem (2.22)–(2.27) we will derive a travelling-wave solution via matched asymptotics, for the regime $v \ll 1$. As is well-known, the travelling-wave exhibited by the thin film spreading down the inclined plane, typically shows a hump near the contact line. Here, surface tension and gravitational forces dominate, while further away from the contact line region surface tension can be neglected and viscous and gravitational forces balance. This suggests the use of singular perturbation methods [21], where solutions close to the leading edge are to be matched with solutions far upstream.

Since we are looking for a travelling-wave solution, we introduce the coordinate $\xi = x - \Gamma_{tw}(t)$, where the contact line is the straight line $\Gamma_{tw}(t) = u_{tw}t$, u_{tw} = constant travelling-wave velocity, and approximate $h(x,y,t)$ by $h_{tw}(\xi)$. Thus

$$v(1+d^2)u_{tw}\,h_{tw}'(\xi) = \frac{d}{d\xi}\left[\left(\frac{1}{B}h_{tw}'''(\xi) - h_{tw}'(\xi) + v\right)(h_{tw}^3(\xi) + h_{tw}(\xi)\,d^2)\right] \tag{3.1}$$

with boundary conditions

$$h_{tw}(0) = 0, \tag{3.2}$$

$$h_{tw}'(0) = -\theta_S - D_1\,v, \tag{3.3}$$

$$\lim_{\xi\to-\infty} h_{tw}(\xi) = 1, \tag{3.4}$$

$$\lim_{\xi\to-\infty} h_{tw}^{(n)}(\xi) = 0, \qquad n \in \mathbb{N}. \tag{3.5}$$

Note that we can integrate (3.1) once, and that the integral is zero as long as we require $h_{tw}'''(\xi)$ and $h_{tw}'(\xi)$ to remain bounded when $\xi \to 0$. This in turn is a result of the particular

choice of the slip condition λ/h (see also Greenspan [7] and Haley & Miksis [20]). On the other hand, we see from the conditions at $-\infty$ that $u_{tw} = 1$.

In the following perturbation analysis we keep d^2 as an independent parameter. Note that, even though d^2 enters the problem as a singular parameter, our subsequent results show that the dependence is only logarithmic, and one can then infer, after a little algebra, that our asymptotic solution remains valid as long as

$$|v \ln(d)| \ll 1$$

is obeyed.

For the inner expansion we write:

$$h_{tw}(\xi; v) = g_0(\xi) + v g_1(\xi) + O(v^2) \tag{3.6}$$

The solutions of the leading order and $O(v)$ problems (see Appendix A) are given by:

$$g_0(\xi) = \frac{C_0}{2}\left(e^{-\sqrt{B}\xi} - e^{\sqrt{B}\xi}\right) + \frac{\theta_S - \sqrt{B}C_0}{\sqrt{B}}\left(1 - e^{\sqrt{B}\xi}\right) \tag{3.7}$$

and

$$\begin{aligned} g_1(\xi) = \frac{m_0}{\theta_S}\Bigg[&(1-y)\left(D_1 + k_3 + \frac{k_1}{2} - \frac{1+d^2}{2m_0 d}\arctan\left(\frac{m_0}{d}\right)\right.\\ &\left.+ \frac{k_1 k_2 m_0}{2d}\arctan(v) + \frac{k_1 m_0^2}{2k_0}\left(\ln(w) - \ln(d^2)\right)\right)\\ &+\frac{k_1}{4}(1-k_2)\left(\ln(w) - \ln(d^2)\right) + \frac{k_1 m_0^2}{k_0} y\ln(y) - \frac{1+d^2}{2m_0 d}\arctan\left(\frac{m_0}{d}\right)\\ &+ \frac{k_1 k_2 m_0}{2d}\arctan(v) - \frac{1+d^2}{2m_0 d}\frac{1}{y}\arctan\left(\frac{v - \dfrac{m_0}{d}}{1 + v\dfrac{m_0}{d}}\right)\Bigg] + k_3\xi \end{aligned}$$

where

$$\begin{aligned} y &= e^{\sqrt{B}\xi}, \qquad k_1 = \frac{1+d^2}{m_0^2 + d^2}, \quad w = m_0^2(1-y)^2 + d^2,\\ m_0 &= \frac{\theta_S}{\sqrt{B}}, \qquad k_2 = \frac{m_0^2 - d^2}{m_0^2 + d^2}, \quad v = \frac{m_0}{d}(1-y),\\ k_0 &= m_0^2 + d^2, \quad k_3 = \frac{m_0^2 - 1}{m_0^2 + d^2}. \end{aligned} \tag{3.8}$$

On the other hand, when ξ is large (i.e. $\xi = \xi^*/v$), we write for the outer expansion

$$h_{tw}(\xi; v) = u_0(\xi^*) + v u_1(\xi^*) + O(v^2). \tag{3.9}$$

The solutions for the corresponding leading and $O(v)$ problems (see Appendix A) are given implicitly:

$$\begin{aligned} u_0(\xi^*) - (1+d^2)\operatorname{arcoth}(u_0(\xi^*)) &= C_1^+ + \xi^* \qquad \text{for} \quad u_0 > 1,\\ u_0(\xi^*) - (1+d^2)\operatorname{artanh}(u_0(\xi^*)) &= C_1^- + \xi^* \qquad \text{for} \quad u_0 < 1, \end{aligned} \tag{3.10}$$

and

$$u_1(\xi^*) = m_1 \frac{du_0}{d\xi^*}. \tag{3.11}$$

Matching to leading order requires $C_0 = 0$, since u_0 remains bounded as $\xi^* \to 0$. Hence, since $g_0 \to \theta_S/\sqrt{B}$ as $\xi \to -\infty$, the integration constants $C_1^{\pm}$ will be matched to

$$C_1^+ = \frac{\theta_S}{\sqrt{B}} - (1+d^2)\,\mathrm{arcoth}\left(\frac{\theta_S}{\sqrt{B}}\right), \tag{3.12}$$

$$C_1^- = \frac{\theta_S}{\sqrt{B}} - (1+d^2)\,\mathrm{artanh}\left(\frac{\theta_S}{\sqrt{B}}\right), \tag{3.13}$$

as $\xi^* \to 0$. When we match to $O(v)$, we have to match $g_1(\xi)$ as $\xi \to -\infty$ with contributions of $O(v)$ from the outer expansion as $\xi^* \to 0$. These are

$$v u_1(\xi^*) + \xi^* \frac{du_0}{d\xi^*}(0). \tag{3.14}$$

We see immediately from (A 7) in Appendix A that, since $du_0/d\xi^* = k_3$ when $\xi^* \to 0$, the second term matches with the last term of g_1, and as the rest of g_1 approaches a constant, that m_1 is determined to be

$$m_1 = \frac{m_0}{\theta_S}\left[\frac{D_1+1}{k_3} + \frac{k_1}{k_3}\left(\frac{1}{2}\left(\ln(k_0) - \ln(d^2)\right) - \frac{d}{m_0}\arctan\left(\frac{m_0}{d}\right)\right)\right] \tag{3.15}$$

Hence, we obtain for the travelling-wave solution to $O(v)$:

$$h_{tw}(\xi) = g_0(\xi) + u_0(v\xi) - m_0 + v\,(g_1(\xi) + u_1(v\xi) - k_3\xi - m_1) + O(v^2). \tag{3.16}$$

For the case $m_0 = \theta_S/\sqrt{B} = 1$ the solution can be given explicitly [25].

3.1 Numerical methods

We solved (3.1)–(3.5) numerically with a pseudo-spectral method based on expansions in Chebyshev-polynomials and, independently, a multiple-shooting code using the package MUMUS developed by Peter Hiltmann at the Technical University of Munich [26].

The semi-infinite domain of the boundary value problem was cut off at $-L$. The choice of L is critical since too small a value (i.e. if $h_{tw}(-L)$ is not yet in the asymptotic regime so that $|h_{tw}(-L)| \gg 1$) may distort the result. On the other hand, large values of the cut-off parameter demand a penalty in time and/or accuracy.

In the multiple-shooting method the third order ODE (3.1) was converted into a first order system and (3.2)–(3.5) provided the necessary boundary conditions. The integration of the initial value sub-problems was performed through an embedded 7/8th-order Runge–Kutta–Fehlberg method. The step-size control of this initial-value solver produced, in effect, a highly adapted grid.

For the pseudo-spectral method (see Canuto *et al.* [27] and Gottlieb & Orszag [28]), we linearly mapped $]-L, 0[$ to $]-1, 1[$ and discretized $h_{tw}(\xi)$ on a fixed grid given by

$$\xi_i := \cos\left(\frac{i\pi}{N}\right), \qquad i = 0, \ldots, N = 2^p, \quad p \in \mathbb{N}.$$

This choice of the grid and the restriction of the number of grid-points N to a power

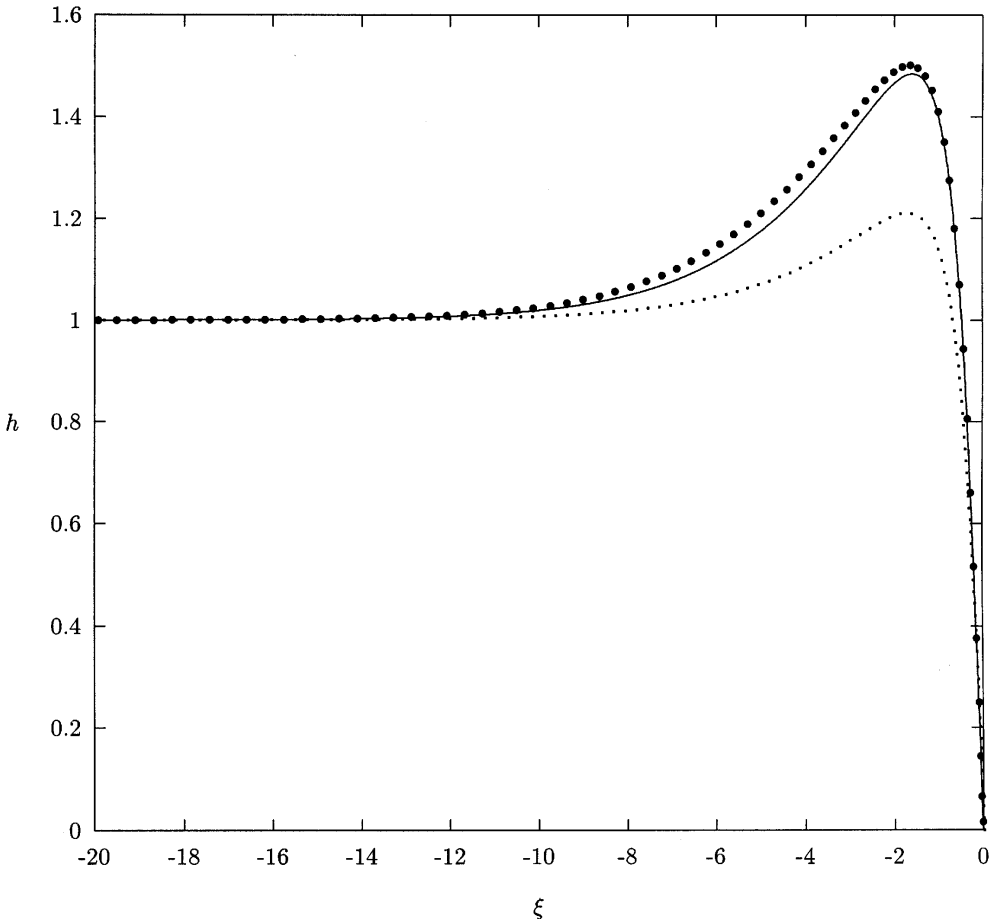

FIGURE 2. Travelling wave solution (outer scale) zeroth-order approximation ($\cdots$), first-order approximation (—), numerical (●), for $\alpha = 0.04$, $v = 0.24$.

of two is mandated by the fast-Fourier transform which is used to perform the actual computation for the Chebyshev-expansions. It exhibits a strong bunching of the grid-points near ± 1, but allocates enough resolution throughout the entire hump region to yield satisfactory results for moderate values of N ($N \geqslant 128$).

3.2 Comparison with the asymptotic solution

For all the comparisons below we used values of parameters obtained from experimentally measured and estimated data. For example, it was found that the fluid depth profile of the spreading thin film showed favourable agreement between the numerical solution and recent experiments [6]. There, the dynamic contact angle model $\langle u, v\rangle|_\Gamma \cdot \boldsymbol{n}_\Gamma = \kappa(\theta - \theta_S)^m$, for the case $m = 3$ was studied as well, but no relevant difference was found when $m = 1$ for the experiments considered. When we chose similar parameter values (for the case $m = 1$) but let α be small, we found excellent agreement of our asymptotic and numerical travelling-wave solutions. Figures 2–3 show typical examples from various

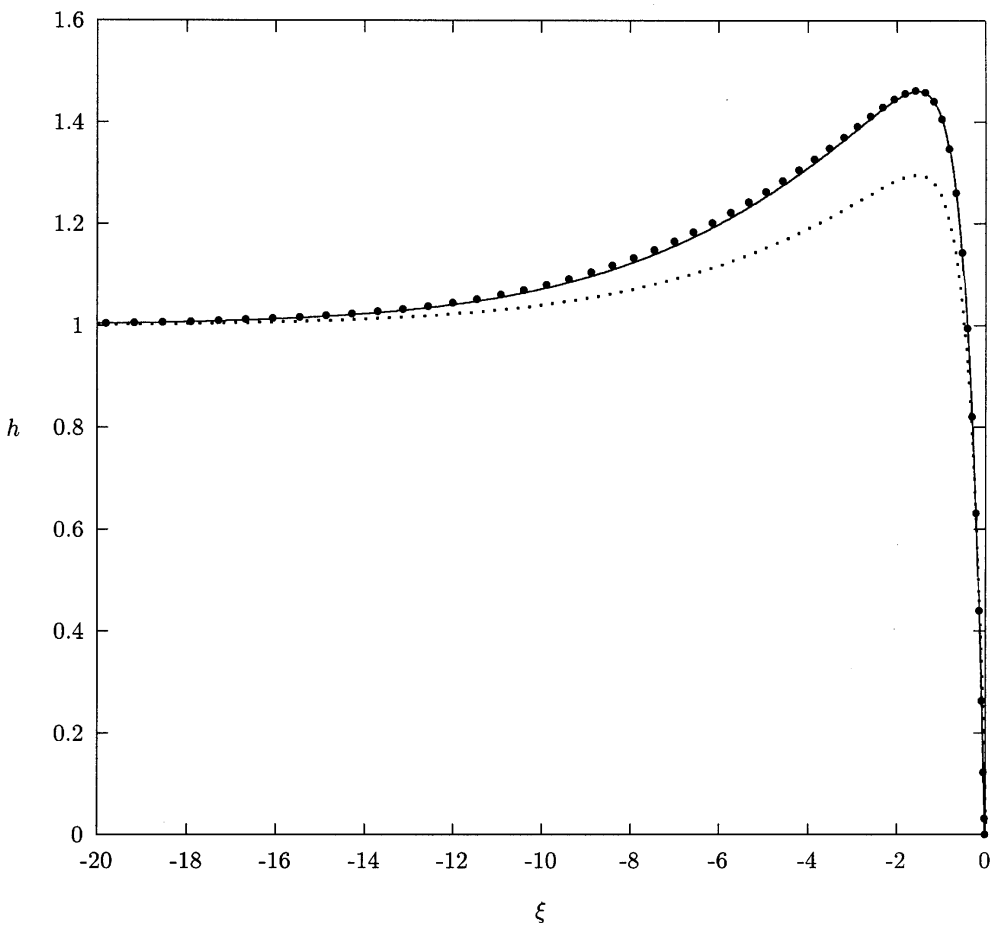

FIGURE 3. Travelling wave solution (outer scale) zeroth-order approximation (· · ·), first-order approximation (—), numerical (●), for $\alpha = 0.02$, $v = 0.15$.

series of comparisons we performed. Here we let the unscaled static contact angle $\theta_S = 0.5$, $D_1 = 1$, $\sqrt{\rho g h_\infty^2/\sigma} = 0.35$, $d^2 = 0.003$, and $v = 0.24$, 0.15 with $\alpha = 0.04$, 0.02, respectively.

Further, we think it is interesting to observe, that the asymptotic solution of the travelling-wave explicitly shows a logarithmically singular behaviour at the contact line as the slip parameter d^2 vanishes. For the same parameter values, except $\alpha = 0.04$ and $v = 0.24$, Figure 4 illustrates this behaviour for both, our asymptotic as well as numerical solution, by depicting the dependence of the maximum height on d^2 in a semi-log diagram. We would like to stress at this point that this is in accordance with numerical results for the precursor model, when the thickness of the precursor b vanishes – see Troian *et al.* [13] and Bertozzi & Brenner [14].

4 Linear stability analysis and long-wave approximation

In this section we will investigate the stability of the travelling-wave solution, by allowing a small deviation of its straight contact line. We are particularly interested in the range

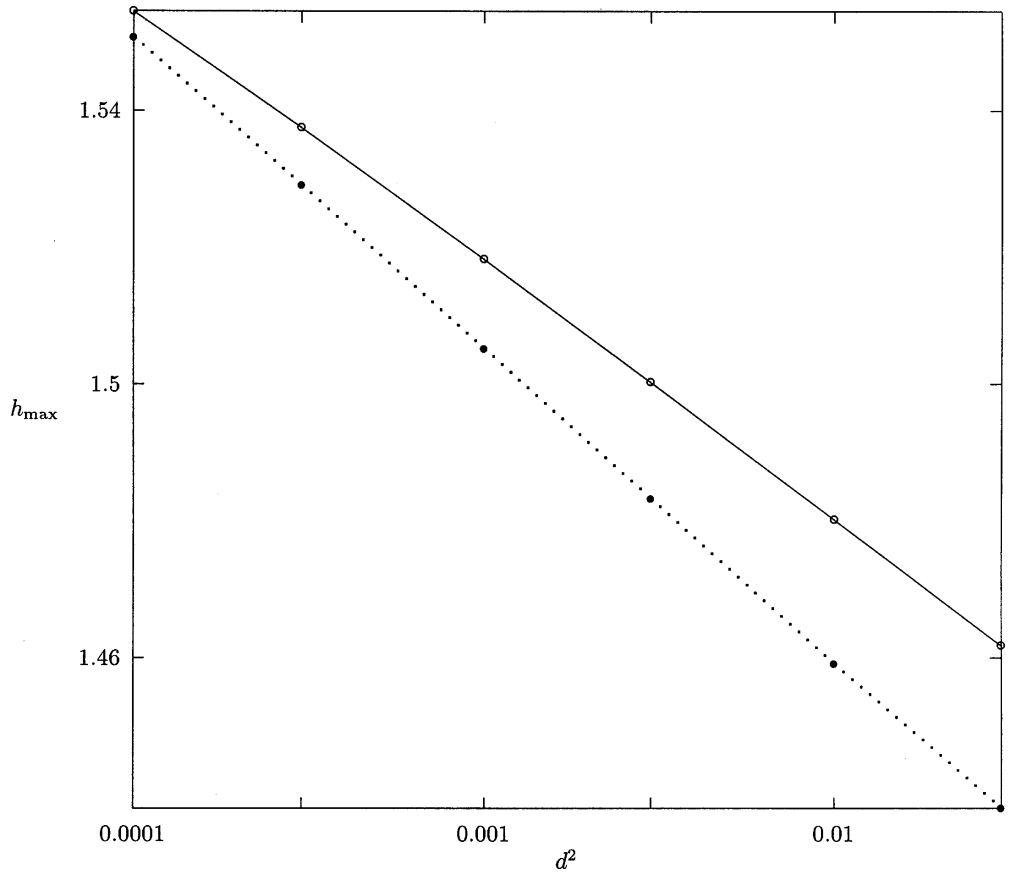

FIGURE 4. $\max_\xi h_{tw}(\xi)$ vs. slip length d^2 in a semi-log diagram, for $\alpha = 0.04$, $v = 0.24$. Values for the numerically computed TW solution (—), and for the asymptotic approximation ($\cdots$).

of values of the parameters, such as α, θ_S, D_1 and configurations thereof, under which the flow remains linearly stable.

According to Bertozzi & Brenner [14], who use a precursor model, there is a critical inclination angle $\alpha^* > 0$ (α^* was estimated to to be between 5 to 10 degrees) below which the flow remains linearly stable, yet experiments due to de Bruyn [4] show that fingers still emerge for angles below α^*. This apparent paradox was studied using a transient growth approach. It is therefore interesting to investigate this problem for the slip model, where slip and contact angles can be prescribed and compared to experimental measurements (e.g. see Johnson *et al.* [6]).

We begin our stability analysis by expressing the perturbations of the contact line, height and contact angle in terms of normal modes as follows:

$$\Gamma(y,t) = \Gamma_{tw}(t) + \delta e^{st+iky}, \tag{4.1}$$

$$h(x,y,t) = h_{tw}(\xi) + \delta h_1(\xi) e^{st+iky}, \tag{4.2}$$

$$\theta(y,t) = \theta_{tw} + \delta\theta_1 e^{st+iky}, \tag{4.3}$$

where $\theta_{tw} = \theta_S + D_1 v$, s is the growth rate and k the wavenumber.

If we now substitute (4.1)–(4.3) into (2.22)–(2.27) we obtain for the leading order problem (3.1)–(3.5) and to $O(\delta)$ the following eigenvalue problem for s, parametrized by the wavenumber k:

$$\frac{d}{d\xi}\left(c_3(h_{tw})\,h_1'''(\xi)\right) + c_2(h_{tw})\,h_1''(\xi) + c_1(h_{tw})\,h_1'(\xi) + c_0(h_{tw})\,h_1(\xi) = 0, \tag{4.4}$$

with boundary conditions

$$h_1(0) = -h_{tw}'(0) = \theta_S + D_1\,v, \tag{4.5}$$

$$h_1'(0) = -h_{tw}''(0) - sD_1v, \tag{4.6}$$

$$\lim_{\xi\to-\infty} h_1(\xi) = 0, \tag{4.7}$$

$$\lim_{\xi\to-\infty} h_1^{(n)}(\xi) = 0 \qquad n \in \mathbb{N}, \tag{4.8}$$

where

$$c_3(h_{tw}) = \frac{1}{B}\left(h_{tw}^3(\xi) + d^2\,h_{tw}(\xi)\right), \tag{4.9}$$

$$c_2(h_{tw}) = -(2k^2 + B)\,c_3(h_{tw}), \tag{4.10}$$

$$c_1(h_{tw}) = -(k^2 + B)\frac{dc_3}{d\xi} + (1 + d^2)v\ \frac{2h_{tw}^2(\xi)}{h_{tw}^2(\xi) + d^2}, \tag{4.11}$$

$$c_0(h_{tw}) = k^2(k^2 + B)\,c_3(h_{tw}) + (1 + d^2)\left[vs + v\frac{d}{d\xi}\left(\frac{2h_{tw}^2(\xi)}{h_{tw}^2(\xi) + d^2}\right)\right]. \tag{4.12}$$

When looking for the eigenvalues with the largest real parts we find, similar to López *et al.* [12], Troian *et al.* [13] and Bertozzi & Brenner [14], that $s(k)$ increases from zero to a maximum value $s_{\max}$ and decreases again to zero at a certain $k = k_z$ as k increases from zero to k_z.

As a check of our calculations, we compare our results for the most unstable mode with recent experimental measurements [6]. We find good agreement, as was found earlier by López *et al.* [24]. For example, for the choice of $\alpha = 0.253$, $\epsilon = 0.328$, $\sqrt{\rho g h_\infty^2/\sigma} = 0.375$, $\theta_S = 0.171$ (unscaled), $D_1 = 1$ and $d^2 = 0.003$, which were determined from the physical data given in Johnson *et al.* [6], we found for the preferred dimensionless wavelength the value of $k_{\max} = 0.38 \pm 0.01$, while Johnson *et al.* [6] measure $0.377 \ldots 0.491$. Note at this point, that similarly good agreement between experimentally observed and theoretically predicted values of the preferred wavelength was found by using the precursor model – see Troian *et al.* [13] and Bertozzi & Brenner [14].

We now wish to study the behaviour of the function $s(k)$ when we change the physical parameters, in particular when we decrease α. We find that $s_{\max}$ also decreases as well as the location of the maximum $k_{\max}$. We are interested in the value of α^* for which $s_{\max}$ reaches zero. This, however, eventually presents a problem in numerical accuracy as α^* and $s_{\max}$ become exceedingly small. We therefore seek the asymptotic behaviour of $s(k)$ for small k, and match this to the numerical solution for larger k.

The assumption that k is small, i.e. the wavelength of the disturbance becomes large, simplifies above eigenvalue problem (4.4)–(4.12) considerably. First, note that k appears in the problem only as k^2, and we thus make the following ansatz:

$$h_1(\xi; k^2) = f_0(\xi) + k^2 f_1(\xi) + O(k^4),$$

and

$$s(k) = k^2 s_1 \tag{4.13}$$

where s_1 is a constant an $k^2 \ll 1$.

If we now substitute this ansatz into (4.4)–(4.12), we obtain to leading order the problem

$$\frac{1}{B} f_0'''(\xi) - f_0'(\xi) = -v \, \frac{2h_{tw}(\xi)(1+d^2)}{(h_{tw}^2(\xi)+d^2)^2} \, f_0(\xi),$$

with boundary conditions

$$\begin{aligned} f_0(0) &= -h_{tw}'(0), \\ f_0'(0) &= -h_{tw}''(0), \\ \lim_{\xi \to -\infty} f_0(\xi) &= 0, \\ \lim_{\xi \to -\infty} f_0^{(n)}(\xi) &= 0. \end{aligned} \tag{4.14}$$

Note that, since

$$\frac{d}{d\xi} \left(\frac{h_{tw}^2(\xi) - 1}{h_{tw}^2(\xi) + d^2} \right) = \frac{2h_{tw}(\xi)(1+d^2)}{(h_{tw}^2(\xi)+d^2)^2} \, h_{tw}'(\xi) \tag{4.15}$$

one can easily see the solution of the problem to be $f_0(\xi) = -h_{tw}'(\xi)$. By making use of this solution, we find to the next order the problem

$$\begin{aligned} &\frac{d}{d\xi} \left[c_3(h_{tw}) \left(\frac{1}{B} f_1'''(\xi) - f_1'(\xi) \right) + v \, \frac{2h_{tw}^2(\xi)(1+d^2)}{h_{tw}^2(\xi)+d^2} \, f_1(\xi) \right] \\ &\quad = \frac{d}{d\xi}(c_3(h_{tw}) \, f_0'(\xi)) + c_3(h_{tw}) \, f_0''(\xi) - (1+d^2) v s_1 \, f_0(\xi) - B c_3(h_{tw}) \, f_0(\xi) \\ &\quad = -\frac{d}{d\xi}(c_3(h_{tw}) \, h_{tw}''(\xi)) - c_3(h_{tw}) \, h_{tw}'''(\xi) + (1+d^2) v s_1 \, h_{tw}'(\xi) + B c_3(h_{tw}) \, h_{tw}'(\xi) \end{aligned} \tag{4.16}$$

with boundary conditions

$$\begin{aligned} f_1(0) &= 0, \\ f_1'(0) &= -D_1 s_1 v, \\ \lim_{\xi \to -\infty} f_1(\xi) &= 0, \\ \lim_{\xi \to -\infty} f_1^{(n)}(\xi) &= 0. \end{aligned} \tag{4.17}$$

If we now integrate over the range of ξ from $-\infty$ to zero and use the boundary conditions for $h_{tw}(\xi)$ and $f_1(\xi)$, we find that the right-hand side of equation (4.16) vanishes, and only the last three terms of the left-hand side remain. This then yields the following formula for s_1:

$$s_1 = \frac{1}{1+d^2} \int_{-\infty}^{0} h_{tw}(\xi) \left(h_{tw}^2(\xi) - 1 \right) \, d\xi \, . \tag{4.18}$$

This we can calculate asymptotically for small v.

4.1 Numerical methods

For the numerical solution of (4.4)–(4.12), we represented the boundary conditions (4.5) and (4.6) by an equivalent pair composed of (4.5) and

$$h_1'(0)(\theta_s + D_1 v) + h_1(0)(h_{tw}''(0) + D_1 sv) = 0. \tag{4.19}$$

Since (4.5) is only a normalization condition for the eigenfunction, we can drop it for the essential numerical calculations, so that the remaining set of equations determines h_1 only up to a constant factor.

We solved the resulting eigenvalue problem as follows. The semi-infinite interval was cut off at $]-L, 0[$, mapped linearly to $]-1, 1[$ and discretized pseudo-spectrally in the same manner as for the travelling-wave solution. Then, standard software (from EISPACK [29]) was used to compute the eigenvalue with the largest real part, which is the dominant growth rate $s(k)$ for the wave number k – see also Canuto *et al.* [27], Gottlieb & Orszag [28] and López *et al.* [12].

The numerical experiments were initially performed on an SGI Indigo workstation in 64-bit double precision (DP) arithmetics. Since it is known from the above analysis that $s(0)$ must be zero, the numerical approximation s_0 for this value can serve as an estimate for the accuracy of our calculations. It turned out that $|s_0|$ decreased with N as long as $N \leqslant 128$, but increased for $N \geqslant 256$. This behaviour is surprising only at first glance, since the accuracy of s is limited by the accuracy to which the fourth order derivatives appearing in (4.4) can be calculated. As a 'rule of thumb', round-off errors tend to be the dominant error contribution if the minimum distance of two adjacent grid points $\Delta_{\min}$ is less than order $\mathrm{eps}^{(1/4)}$, where the machine precision eps is about 10^{-16} for DP. Since

$$\Delta_{\min} = \left|\cos\left(\frac{\pi}{N}\right) - 1\right| \approx \frac{\pi^2}{2N^2},$$

we get

$$N \geqslant \frac{\pi}{\sqrt{2\,\mathrm{eps}^{\frac{1}{4}}}} \approx 222$$

as the threshold above which round-off errors must be expected to corrupt the numerical data. This value fits in nicely with our observations.

Unfortunately, the accuracy obtained for the highest possible $N = 128$ was not sufficient to generate reliable $s(k)$ plots for all interesting values of α. Especially near the point of stability transition, the quality of the plots was so poor that no agreement with the long-wave predictions was achieved.

To enable the use of higher resolution, i.e. higher values of N, we opted for higher precision arithmetics by using the Quadruple Precision (QP) floating point libraries of a SUN workstation. Since these are implemented in software, the pseudo-spectral code had to be redesigned to keep the computation time acceptable. The precision sensitive part turned out to be problem independent and could be done once and for all for each value of N, such that it could be retrieved for the problem-specific calculations, which were carried out in hardware-supported, i.e. fast, DP arithmetics. Except for the one-time generation of the problem independent QP data, and the fact that computing the eigenvalues of the

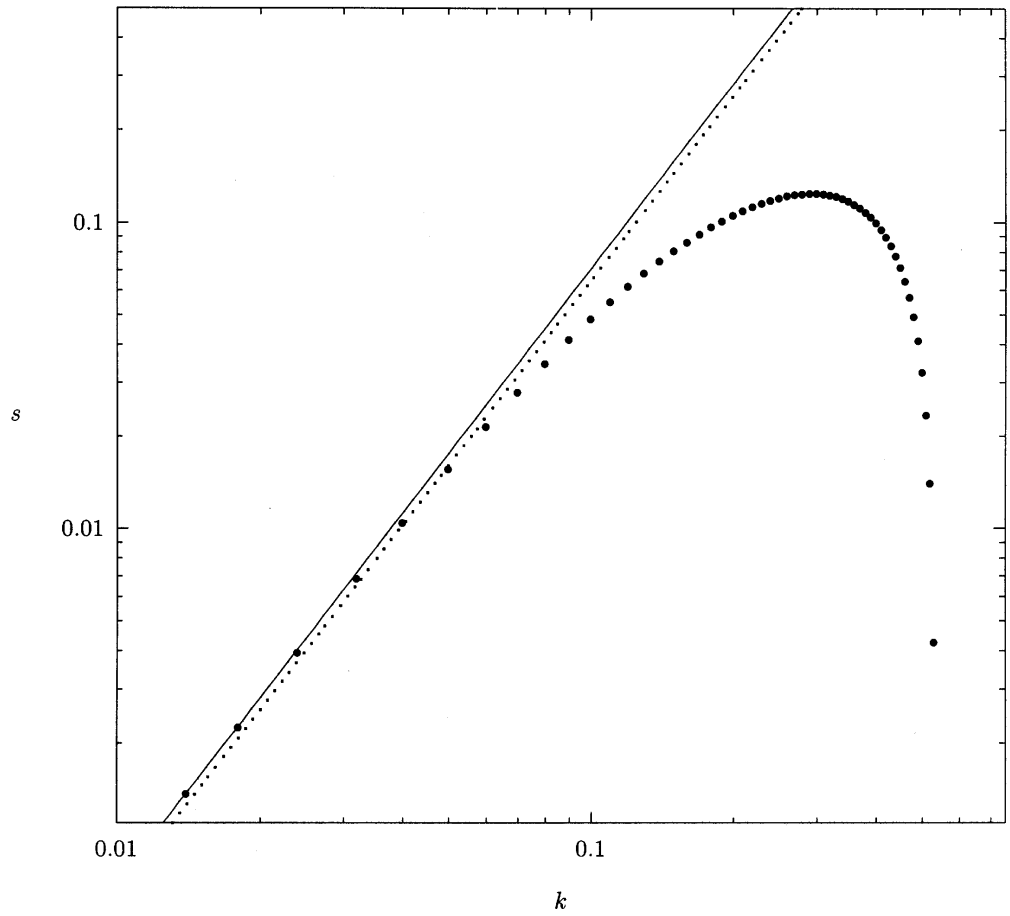

FIGURE 5. Growth rate s vs. wavenumber k on log–log scales for $\alpha = 0.03$, $v = 0.19$. Long-wave approximation: numerical (—), asymptotical ($\cdots$), numerical: (●).

matrices for larger N took considerably longer, no extra penalty in computation time was paid. For further details, see Münch [30].

5 Numerical and asymptotic results

The growth rate $s(k)$ is shown in Figure 5, for $\sqrt{\rho g h_\infty^2/\sigma} = 0.35$, $d^2 = 0.003$, $\theta_S = 0.5$ (unscaled), $\alpha = 0.03$, $v = 0.19$ and $D_1 = 1$, and compared to results from long-wave analysis, by using both the numerical and the asymptotic travelling-wave solution to determine s_1. To illustrate that the approximation is very good for small k, Figure 5 depicts the log-log comparison.

As the inclination angles get smaller, the maximum growth rate $s_{\max}$ decreases, as well as the maximum wavenumber $k_{\max}$. However, a similar scenario can be seen when the contact angle is varied. This behaviour can be seen in Figures 6–7, where we fix α in each figure and plot the growth rate versus wavenumber for various $\theta_S/\sqrt{B}$, leaving the remaining parameters as in figure 5. We observe, that for fixed α the point $(k_{\max}, s_{\max})$

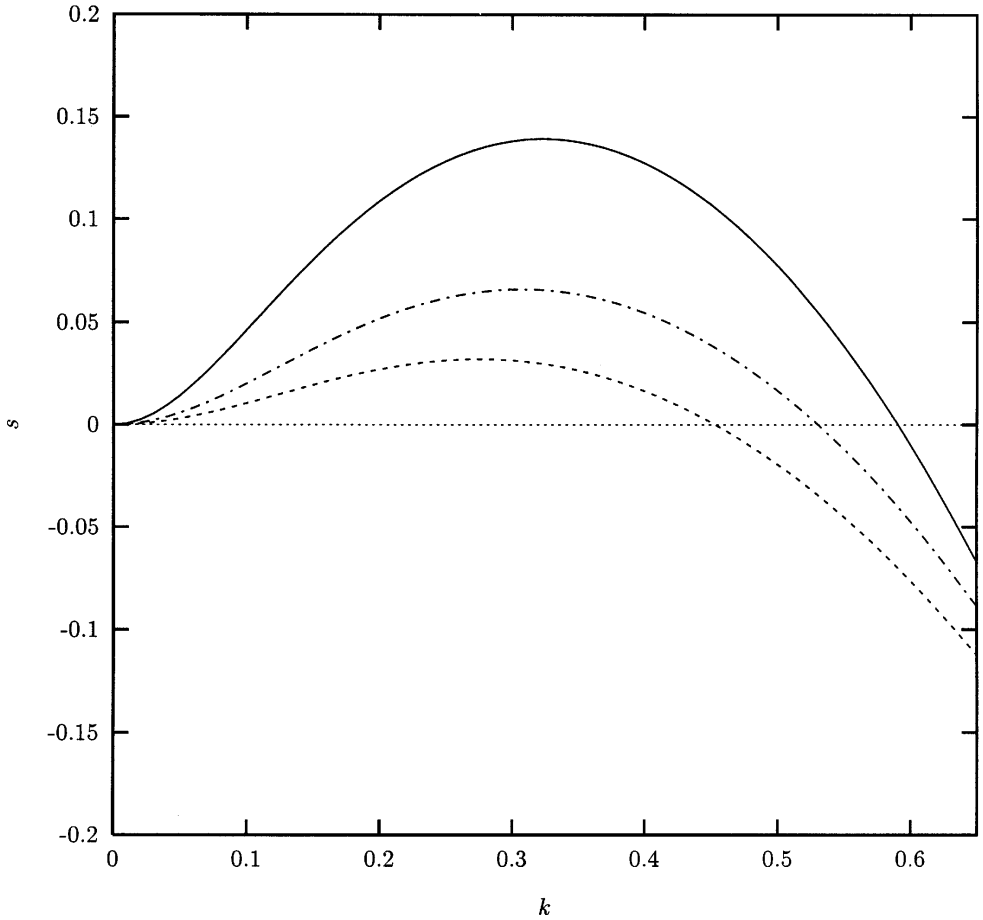

FIGURE 6. Growth rate s vs. wavenumber k for $\theta_s/B^{1/2} = 1.428$ (—), 1 (— · —), 0.714 (— — —), $\alpha = 0.06$, $v = 0.31$.

moves further towards the origin as $\theta_S/\sqrt{B}$ get smaller, as was the case for fixed $\theta_S/\sqrt{B}$ and decreasing α.

This leads us to the problem to determine, for a fixed θ_S the inclination angle α for which the flow is linearly stable. Here, we take up the apparent paradox exposed by Bertozzi & Brenner [14], who studied the problem of linear stability and found so large a value of α^*, that it contradicted experimental observations. They used a precursor model, which is the limiting case of completely wetting fluids. We find in our analysis, that to each fixed θ_S there is a critical α^*. The value of α^* decreases as θ_S increases. However, one can also observe from Figures 2–3 that the hump height decreases as α decreases, as does the maximum growth rate in the corresponding curves of Figures 6–7. We then tried to relate vanishing of the hump with the linear stability of the flow. In Figure 8 we compare the function for the critical α^*, for which the flow becomes stable, with the critical α where the hump vanishes. We observe that, indeed, the flow stabilizes at a finite α^*, which decreases though as θ_S increases. A similar behaviour is seen for the vanishing of the hump. There is considerable discrepancy between the critical α, where the hump vanishes

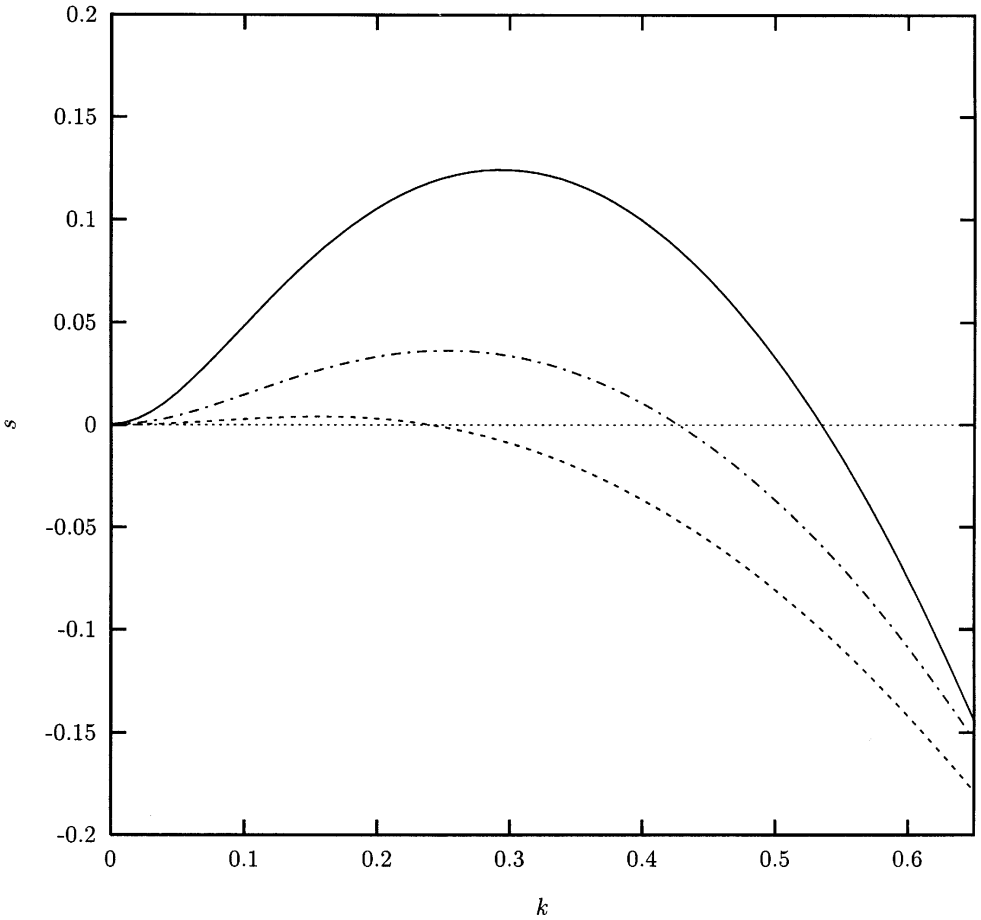

FIGURE 7. Growth rate s vs. wavenumber k for $\theta_s/B^{1/2} = 1.428$ (—), 1 (— · —), 0.714 (— — —), $\alpha = 0.03$, $v = 0.19$.

and where the flow is stable, which is expected from formula (4.18). Interestingly though, as θ_S increases, these curves move closer together. This behaviour, to our knowledge has not been observed before, and it would be interesting to obtain experimental comparisons. We also note here, that the influence of varying D_1 is very small for small θ_S, as can be seen from Figure 9, but acts as a more destabilizing contribution as θ_S increases.

To predict the behaviour for large θ_S, we would eventually have to leave the lubrication limit. However, we think the indication that the discrepancy between these two curves decreases, while both curves approach ever smaller values of α^*, may hint towards different underlying physical mechanisms as the dominant causes of the instability. It should therefore be interesting to investigate these curves as θ_S increases, and determine if and for which θ_S linear stability theory is sufficient to describe the instability.

For small θ_S though there remains a problem. For example, Jerrett & de Bruyn [3] use Heavy Mineraloil (HMO) on plexiglass. From the typical roughness of plexiglass, which is about 0.1–1 μm, we can infer a value for d^2 of about 10^{-3}–10^{-5}. We calculate, given

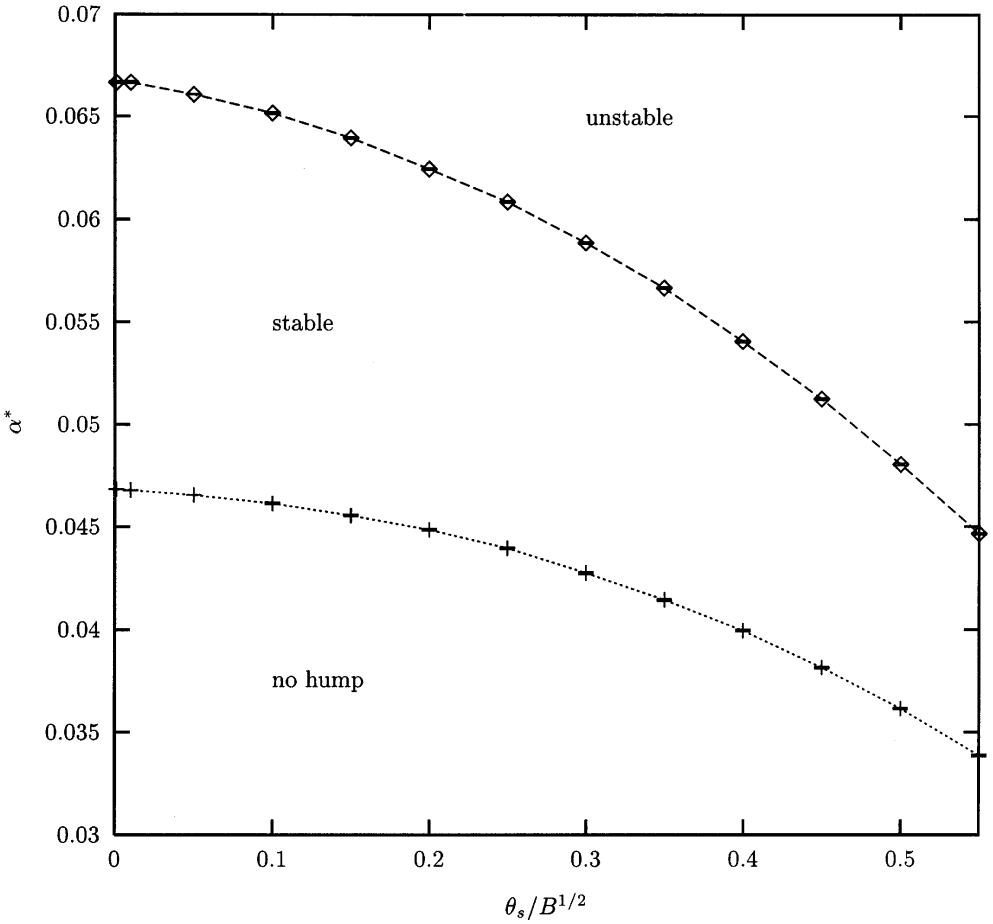

FIGURE 8. Transition curves for linear stability and vanishing of the hump for various $\theta_s/B^{1/2}$, $d^2 = 0.003$, $D_1 = 1$, $(\rho g h_\infty^2/\sigma)^{1/2} = 0.5$.

their measured quantities, a critical α^* of about 0.066, i.e. 3.8°. However, Jerrett & de Bruyn observe instabilities down to 2°.

6 Conclusions

In this work we have studied various aspects of a thin fluid film spreading down an inclined plane, in particular for small inclination angles, by using a slip model.

We derived a matched asymptotic solution for the travelling-wave, which shows excellent agreement with numerical calculations. Furthermore, it explicitly showed a logarithmically singular dependence on the slip parameter. We then studied the linear stability of the travelling-wave. We found that for small wavenumbers a long wave approximation yields an expression for the growth rates that depends only on the slip parameter and the solution to the travelling-wave, and compares well with numerical solutions in this regime.

These results are in accordance with numerical studies for the precursor model, i.e.

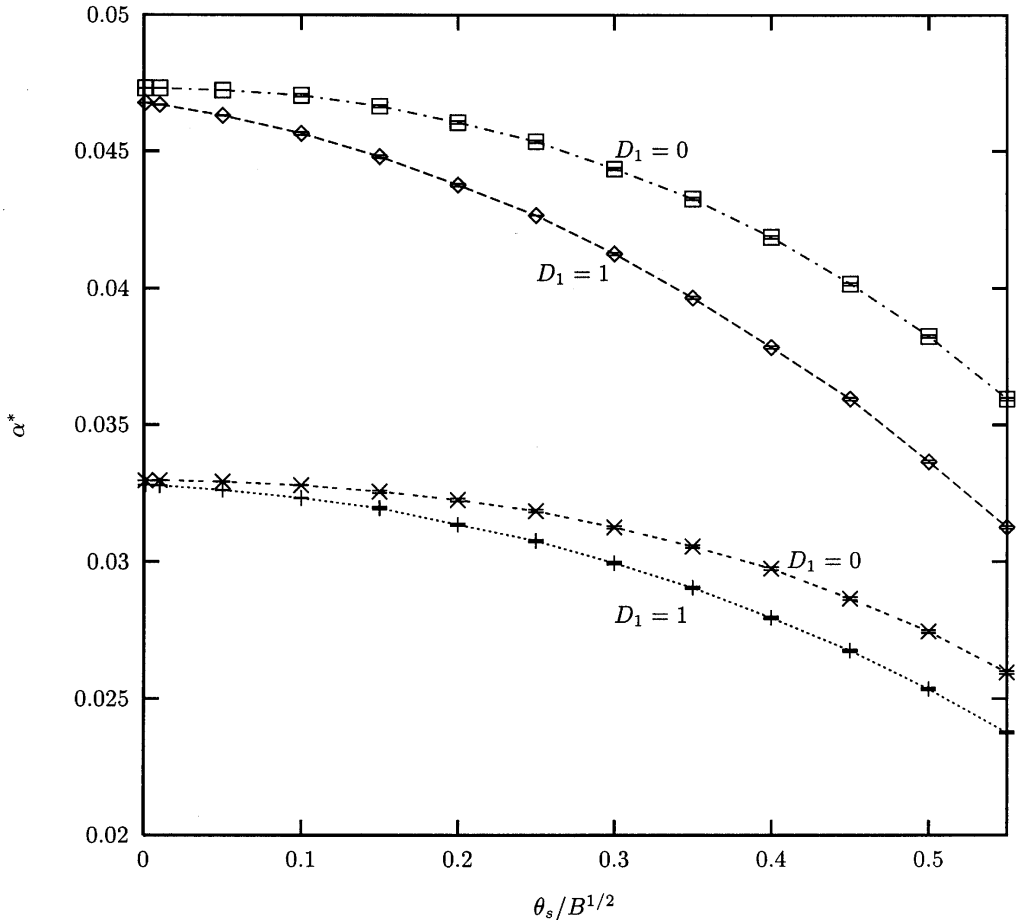

FIGURE 9. Comparison of transition curves for linear stability and vanishing of the hump for various $\theta_s/B^{1/2}$, $d^2 = 0.003$, $(\rho g h_\infty^2/\sigma)^{1/2} = 0.35$, $D_1 = 0,\ 1$.

logarithmically singular dependence of the height on the precursor thickness, long wave approximation for small wavenumbers, as well as the favourable agreement of the predicted wavelength of the instability with experimental data, in spite of the different approaches to model the contact line region, reflecting a quite different understanding of the underlying physics there.

However, only when the ratio of $\theta_S/\sqrt{B}$ becomes small do we recover the result of Bertozzi & Brenner [14], and find critical values for the inclination angle below which all normal modes are stable, and which are in contradiction to some experimental observation. Furthermore, by increasing $\theta_S/\sqrt{B}$ we find that these critical values decrease as well as those critical α^* for which the hump of the travelling-wave vanishes.

Additionally, we saw that these two transition curves seem to move closer together as $\theta_S/\sqrt{B}$ increases, and we have indications from present numerical as well as asymptotical calculations (to be published), that they eventually merge when $\theta_S/\sqrt{B} = 1$. We also investigate presently the possible connection of this observation with the negligible influ-

ence of the inclination angle on the preferred wavelength when $\theta_S/\sqrt{B} > 1$, as can be seen in Figures 6–7 when $\theta_S/\sqrt{B} = 1.428$.

Another important parameter which needs to be studied more closely is the slip parameter d^2. While we can see in our ongoing analysis that the most unstable mode has negligible dependence on d^2 for large inclination angles, as was also seen for the precursor model, here we also see the same effect for the case when $\theta_S/\sqrt{B} > 1$. We have indications that only in the regime of small α and small $\theta_S/\sqrt{B}$ is the choice of d^2 crucial, since for smaller d^2 the transition curves in Figures 8 and 9 will qualitatively remain the same but with lower values for the respective critical α's.

Bertozzi & Brenner [14] treated their problem by using the method of transient growth, resulting from a disturbance in the precursor film. Interestingly, our present studies (to be published) also show, similar to the problem treated in Bertozzi & Brenner [14], that large amplification of variations in the slip parameter over a finite interval can be observed. Further, we also have indications, by performing a weakly nonlinear stability analysis, that this amplification of the slip variation is sufficient to induce destabilization below α^*.

Acknowledgements

We would like to thank J. D. Cole, A. Bertozzi and B. Tilley for stimulating discussions on various aspects of our investigations. We would also like to thank the referees for helpful comments. We thank FORTWHIR for financial support and also gratefully acknowledge the use of Maple.

Appendix A

The leading order and $O(v)$ boundary value problems are:

$$g_0'''(\xi) - Bg_0'(\xi) = 0, \tag{A 1}$$

$$g_0(0) = 0, \tag{A 2}$$

$$g_0'(0) = -\theta_S, \tag{A 3}$$

and

$$g_1'''(\xi) - Bg_1'(\xi) = -B\frac{g_0^2(\xi) - 1}{g_0^2(\xi) + d^2}, \tag{A 4}$$

$$g_1(0) = 0, \tag{A 5}$$

$$g_1'(0) = -D_1, \tag{A 6}$$

$$u_0{}'(\xi^*) = \frac{u_0{}^2(\xi^*) - 1}{u_0{}^2(\xi^*) + d^2}, \tag{A 7}$$

$$u_0(-\infty) = 1, \tag{A 8}$$

and

$$u_1'(\xi^*) = 2\,u_1(\xi^*)\,u_0(\xi^*)\frac{1 + d^2}{(u_0{}^2(\xi^*) + d^2)^2}, \tag{A 9}$$

$$u_1(-\infty) = 0 \tag{A 10}$$

Note that by integrating (A 9) and using (A 7), we obtain (3.11). Note further that alternatively we can also express u_0 as a series expansion for $\xi^* \to 0$, i.e.

$$u_0(\xi^*) = \sum_{n=0}^{\infty} \frac{c_n}{n!} \left(e^{\frac{2\xi^*}{1+d^2}} - 1 \right)^n, \tag{A 11}$$

with

$$c_n = \frac{d^n u_0}{dz^n}(1), \quad \text{where} \quad z = e^{\frac{2\xi^*}{1+d^2}}. \tag{A 12}$$

References

[1] Huppert, H. E. (1982) Flow and instability of a viscous current down a slope. *Nature* **300**, 427–429.

[2] Silvi, N. & Dussan, E. B. (1985) On the rewetting of an inclined solid surface by a liquid. *Phys. Fluids* **28**(1), 5–7.

[3] Jerett, J. M. & Bruyn, J. R. (1992) Fingering instability of a gravitationally driven contact line. *Phys. Fluids A* **4**(2), 234–242.

[4] de Bruyn, J. R. (1992) Growth of fingers at a driven three-phase contact line. *Phys. Rev. A* **46**(8), R4500–R4503.

[5] Schwartz, A. M. & Tejada, S. B. (1972) Studies of dynamic contact angles on solids. *J. Colloid & Interface Sci.* **38**(2), 359–375.

[6] Johnson, M. F. G., Schluter, R. A., Miksis, M. J. & Bankoff, S. G. (1996) Preprint. Measurement of wavelength, dynamic contact angles, front velocity and shape of rivulets on an inclined plate by fluorescent imaging.

[7] Greenspan, H. P. (1978) On the motion of a small viscous droplet that wets a surface. *J. Fluid Mech.* **84**, 125–143.

[8] Hocking, L. M. (1990) Spreading and instability of a viscous fluid sheet. *J. Fluid Mech.* **211**, 373–392.

[9] Cazabat, A. M. (1991) Wetting films. *Advances in Colloid and Interface Science* **34**, 72–88.

[10] Goodwin, R. & Homsy, G. M. (1991) Viscous flow down a slope in the vicinity of a contact line. *Phys. Fluids A* **3**(4), 515–528.

[11] Hocking, L. M. & Miksis, M. J. (1993) Stability of a ridge of fluid. *J. Fluid Mech.* **247**, 157–177.

[12] López, P. G., Bankoff, S. G. & Miksis, M. J. (1996) Non-isothermal spreading of a thin liquid film on an inclined plane. *J. Fluid Mech.* **324**, 261–286.

[13] Troian, S. M., Herbolzheimer, E., Safran, S. A. & Joanny, J. F. (1989) Fingering instabilities of driven spreading films. *Europhys. Lett.* **10**(1), 25–30.

[14] Bertozzi, A. L. & Brenner, M. P. (1997) Linear stability and transient growth in driven contact lines. *Phys. Fluids* **9**(3), 530–539.

[15] Dussan, E. B. (1976) The moving contact line: The slip boundary condition. *J. Fluid Mech.* **77**, 665–684.

[16] Neogi, P. & Miller, C. A. (1983) Spreading kinetics of a drop on a rough solid surface. *J. Colloid & Interface Sci.* **92**(2), 338–349.

[17] Beavers, G. S. & Joseph, D. D. (1967) Boundary conditions at a naturally permeable wall. *J. Fluid Mech.* **30**, 197–207.

[18] Taylor, G. I. (1971) A model for the boundary condition of a porous material. Part 1. *J. Fluid Mech.* **49**, 319–326.

[19] Richardson, S. (1971) A model for the boundary condition of a porous material. Part 2. *J. Fluid Mech.* **49**, 327–336.

[20] Haley, P. J. & Miksis, M. J. (1991) The effect of the contact line on droplet spreading. *J. Fluid Mech.* **223**, 57–81.

[21] Kevorkian, J. & Cole, J. D. (1986) *Multiple Scale and Singular Perturbation Methods*, Springer-Verlag.

[22] Spaid, M. A. & Homsy, G. M. (1995) Stability of Newtonian and viscoelastic contact lines. Preprint, Department of Chemical Engineering, Stanford University.

[23] Blake, T. D. & Haynes, J. M. (1969) Kinetics of liquid/liquid displacement. *J. Colloid Interface Sci.* **30**, 421–423.

[24] López, P. G., Miksis, M. J. & Bankoff, S. G. (1997) Inertial effects on contact line instability in the coating of a dry inclined plate. *Phys. Fluids* **9**(8), 2177-2183.

[25] Wagner, B. A. (1999) *Perturbation techniques and similarity analysis for the evolution of interfaces in diffusion and surface tension driven problems.* Habilitationsschrift, Zentrum Mathematik, TU München, Munich, Germany.

[26] Hiltmann, P. (1989) *Numerische Lösung von Mehrpunkt-Randwertproblemen und Aufgaben der optimalen Steuerung mit Steuerfunktionen über endlichdimensionalen Räumen.* PhD thesis, TU München, Mathematisches Institut, Munich, Germany.

[27] Canuto, C., Hussaini, M. Y., Quarteroni, A. & Zang, T. A. (1987) *Spectral Methods in Fluid Dynamics.* Series in Computational Physics. Springer-Verlag.

[28] Gottlieb, D. & Orszag, S. A. (1977) *Numerical Analysis of Spectral Methods: Theory and Applications.* Regional Conference Series in Applied Mathematics 26. SIAM.

[29] Smith, B. (1976) *Matrix Eigensystem Routines: Eispack Guide.* Springer-Verlag.

[30] Münch, A. (1998) *Untersuchung der Fingerinstabilität einer sich auf einer schwach geneigten Ebene ausbreitenden Flüssigkeitsschicht*. PhD Thesis, Zentrum Mathematik, TU München, Munich, Germany.